



Unveiling the Corrosion Inhibition Mechanism of Thiazole and Benzo[d]thiazole Gemini Surfactants Using Experimental and Theoretical Approaches

Samir A. Abd El-Maksoud^{1,*}, Mohamed A. Migahed², Mahmoud M. Gouda¹ and Farid I. El-Dossoki¹

¹ Chemistry Department, Faculty of Science, Port-Said University, Port Said 42521, Egypt,

² Petroleum Applications Department, Egyptian Petroleum Research Institute (EPRI), Cairo-Egypt.

*Corresponding author: samirabdelhady@yahoo.com

ABSTRACT

This study investigates the corrosion inhibition performance of two cationic Gemini surfactants related to thiazole and benzo[d]thiazole on AISI 1015 carbon steel in HCl solution using gravimetric weight loss, electrochemical impedance spectroscopy (EIS), potentiodynamic polarization (PDP), and quantum chemical calculations. The adsorption behavior was analyzed and found to follow the Langmuir adsorption isotherm model. The thermodynamic and kinetic parameters for both corrosion and adsorption reactions suggest mixed physical and chemical adsorption. Electrochemical results indicate that both inhibitors TAC 12 and TBC 12 significantly reduce corrosion rate by forming a protective adsorbed film on the steel surface, with inhibition efficiency reaching 87-89% at 50 ppm, where TBC 12 provides a more stable and insulating film over time compared to TAC 12. Potentiodynamic polarization studies confirm that cationic Gemini surfactants inhibit both cathodic and anodic reactions with a dominant cathodic inhibition mechanism. Additionally, quantum chemical calculations and molecular dynamics simulations reveal strong interactions between the inhibitor molecules and the steel surface, validating the experimental findings. Furthermore, the addition of inorganic salts such as MnCl₂, CuCl₂, and CoCl₂ enhanced the inhibition efficiency through a synergistic effect. Electrochemical studies indicate that salts facilitate cooperative adsorption, improving surface coverage and stabilizing the protective film. Among the tested salts, CuCl₂ exhibited the most significant enhancement due to its strong interaction with the inhibitor and metal surface. Overall, the results demonstrate that TAC 12 and TBC 12 are efficient corrosion inhibitors for steel, providing insights into their adsorption mechanism and potential industrial applications.

Keywords: corrosion inhibition, electrochemical studies, adsorption isotherm, quantum chemical calculations

1. INTRODUCTION

Carbon steel is a cornerstone material in modern science, technology, and industry due to its remarkable strength, affordability, and versatility [1-2]. It plays a pivotal role in applications ranging from pipelines and machinery to tools and construction, making it indispensable across numerous sectors [3]. However, despite its widespread use, carbon steel faces a significant challenge: its susceptibility to corrosion, particularly in acidic environments commonly encountered in closed systems such as industrial boilers, heat exchangers, and storage tanks [4-6]. This vulnerability undermines structural integrity, escalates maintenance costs, and poses safety risks, making corrosion a critical issue that demands effective mitigation strategies [7-8].

Among the various approaches to combat corrosion, the use of tailored corrosion inhibitors has emerged as one of the most effective and practical solutions [9]. These inhibitors interact with the metal surface, reducing the rate of corrosive reactions and enhancing the material's durability. Gemini cationic surfactants have gained significant attention due to their superior performance in acidic environments [10]. Unlike traditional cationic surfactants, Gemini surfactants possess a unique dual-head and dual-tail molecular structure that facilitates stronger adsorption onto metal surfaces, forming a compact and stable protective layer [11-14]. This distinctive structure improves corrosion inhibition efficiency, and reduces the required concentration, making them a cost-effective choice for industrial applications [15-16].

Recent advancements in corrosion inhibition research have focused on functionalizing Gemini cationic surfactants with heterocyclic groups, such as thiazole and benzothiazole, to enhance their performance further [17]-[20]. These functional groups, rich in nitrogen and sulfur atoms, provide multiple active sites for adsorption and form strong coordination bonds with the metal surface [21]. The resulting protective film is robust, stable, and water-repellent, shielding the metal from corrosive agents. Additionally, the incorporation of transition metal ions and the influence of ionic strength in the surrounding environment have significantly impacted these surfactants' adsorption and inhibition efficiency [22-24].

This paper explores the corrosion inhibition potential of Gemini cationic surfactants, with a focus on their functionalization with thiazole and benzo[d]thiazole groups. It also examines the role of environmental factors in optimizing their performance, such as temperature, ionic strength, and the presence of transition metal ions. These examinations were addressed by using individual methods or a combination of the following approaches; Gravimetric analysis, potentiodynamic polarization (PDP), electrochemical impedance (EIS), scanning electron microscope (SEM), electron dispersive X-ray (EDX), fourier transform infrared microscope (FTIR) and computational density functional theory (DFT). By leveraging the unique properties of these advanced surfactants, this study aims to contribute to the development of cost-effective, efficient, and environmentally friendly corrosion inhibitors for carbon steel in acidic closed systems.

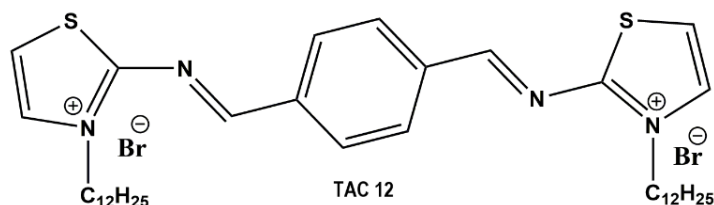
2. Experimental section

2.1 Materials and Solutions

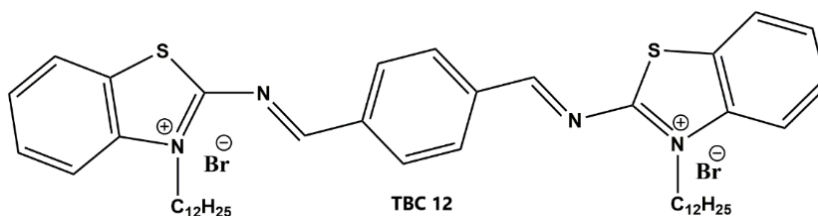
The AISI 1015 carbon steel samples used in this study were composed of C (0.14%), Cr (0.10%), Ni (0.10%), Si (0.024%), Mn (0.05%), P (0.05%), and Fe (balance). This composition was consistently employed across all chemical and electrochemical measurements. Before testing, the carbon steel surface was prepared sequentially polishing with abrasive papers of grit sizes 800, 1000, and 1200 to achieve a uniform finish. The polished electrode and specimens were then thoroughly rinsed with double-distilled water, cleaned with acetone, and dried using absorbent filter paper to ensure a pristine surface.

All chemicals used in this study were procured from Sigma-Aldrich, a globally recognized supplier headquartered in the United States. These chemicals, including hydrochloric acid (37%) and acetone (99.9%), were of analytical grade, eliminating the need for further purification. Additionally, cobalt chloride, manganese chloride, and copper chloride salts with a purity of 98% were employed in the experiments.

The corrosion inhibition experiments were conducted in hydrochloric acid solutions without and with varying concentrations of **TAC 12** and **TBC 12** cationic Gemini surfactants. The molecular structures of these surfactants, synthesized in our laboratory following established protocols [25-26], are illustrated in **Structures 1** and **2**.



Structure 1 The molecular structure of **TAC 12** cationic Gemini surfactants



Structure 2 The molecular structure of **TBC 12** cationic Gemini surfactants

The corrosive solutions were freshly prepared by diluting high-purity concentrated hydrochloric acid with double-distilled water (DCT4/DCT10 - $\kappa_s = 2.5 \mu\text{S}/\text{cm}$, Chem-Tech, Egypt). The inhibitors were utilized at concentrations ranging from 5 to 50 ppm to evaluate their corrosion inhibition efficiency. Additionally, salt solutions of manganese chloride (MnCl_2), copper chloride (CuCl_2), and cobalt chloride (CoCl_2) were added to the corrosive solution in concentrations varying from 10 to 90 ppm to investigate their effects on the corrosion behavior and inhibition performance of both inhibitors.

2.2 Gravimetric analysis

The prepared AISI 1015 carbon steel samples ($2.0 \times 2.0 \times 0.2 \text{ cm}$) were weighed using a USS-DBS10 digital analytical balance (readability: 0.1 mg, U.S. Solid, USA). The specimens were immersed in hydrochloric acid solutions containing varying concentrations of **TAC 12** and **TBC 12** cationic Gemini surfactants for 48 hours at controlled temperatures (30°C to 50°C) using a thermostat water bath (Avantor, VWR, USA). Samples were removed every eight hours, cleaned, dried, and reweighed three times, with the average final weight recorded for accuracy.

2.3 Electrochemical techniques

The corrosion inhibition efficiency was evaluated using a high-performance potentiostat/galvanostat/ZRA (Reference 3000, Gamry Instruments, USA) with a three-electrode system. The setup included a saturated calomel electrode (SCE) as the reference, a platinum electrode as the counter, and an AISI 1015 carbon steel plate (surface area equals 1 cm^2) as the working electrode. The carbon steel plate, attached to a copper rod for electrical conductivity, was encased in a Teflon holder and sealed with epoxy resin. The working electrode was immersed in the corrosive medium for 20 minutes to

stabilize the open-circuit potential (E_{ocp}) before measurements [27]. Electrochemical impedance spectroscopy (EIS) was conducted over a frequency range of 100 kHz to 0.2 Hz using a 10 mV amplitude at (E_{ocp}), with impedance data analyzed using Echem Analyst software and equivalent circuit models. Potentiodynamic polarization curves were recorded by scanning the potential ± 250 mV relative to (E_{ocp}) at a scan rate of 1 mV/s, starting from the cathodic to the anodic region. This approach provided precise insights into the electrochemical behavior and inhibition performance of the **TAC 12** and **TBC 12** cationic Gemini surfactants.

2.4 Computational quantum chemistry

Quantum simulations were conducted using Gaussian 9.0 software to assess the impact of molecular structure on inhibition efficiency. Geometry optimization was performed using the B3LYP hybrid functional with the 6-31G (d,p) basis set [28]. The Gauss View program was used to analyze the energies of the highest occupied molecular orbital (E_{HOMO}), the lowest unoccupied molecular orbital (E_{LUMO}), and the energy gap (ΔE).

3. RESULTS AND DISCUSSION

3.1 Gravimetric Analysis

The corrosion rate of AISI 1015 carbon steel samples immersed into 1 M hydrochloric acid solution without and with the examined inhibitors **TAC 12** and **TBC 12** at different temperatures (303-323 K) and concentrations (5-50 ppm) was summarized in **Table (1)**. The corrosion rate and inhibitory efficiency of both cationic Gemini surfactants were calculated as follows **Eq. (1)** and **(2)**;

$$C.R. = \frac{\Delta W}{A \times t} \quad (1)$$

$$IE \% = \left[1 - \frac{C.R._{inh.}}{C.R._b} \right] \times 100 \quad (2)$$

Where; ΔW is the weight loss of carbon steel specimens, A is the total superficial area, t is the immersion time, $C.R._{inh.}$ is the corrosion rate of carbon steel in the inhibitor solution, and $C.R._b$ is the corrosion rate of carbon steel in the blank solution.

The inhibition efficiencies of **TAC 12** and **TBC 12** increased with concentration, indicating enhanced surface coverage [29]. At 30°C, **TBC 12** achieved an inhibition efficiency of 85.07% at 50 ppm, compared to 80.48% for **TAC 12** at the same concentration. At 50°C, **TBC 12** maintained a higher efficiency (77.68% at 50 ppm) than **TAC 12** (70.79% at 50 ppm), demonstrating better thermal stability [30]. Both surfactants exhibited decreased inhibition efficiency with increasing temperature, attributed to the partial desorption of inhibitor molecules from the steel surface [31]. However, **TBC 12** showed a slower decline in efficiency, suggesting stronger adsorption and a more robust protective film than **TAC 12**. The benzo[d]thiazole moiety in **TBC 12** enhances π -electron interactions and hydrophobic effects, contributing to its superior adsorption and inhibition performance [30-32]. The corrosion rate of steel and the corrosion inhibition of **TAC 12** cationic Gemini surfactant are shown in **Fig. (1)**.

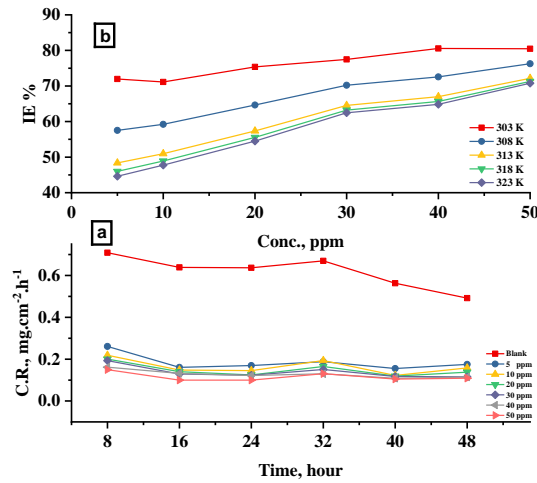


Fig (1): (a) The corrosion rate of AISI 1015 carbon steel in 1M HCl solution without and with the addition of different concentration of **TAC 12** inhibitor (b) The corrosion inhibition efficiency of **TAC 12** under the influence of time.

Table 1: Gravimetric data of AISI 1015 carbon steel immersed in 1 M HCl solution without and with various concentrations of **TAC 12** and **TBC 12** at different temperatures

Soln. Comp.	Temp.	T = 303 K		T = 308 K		T = 313 K		T = 318 K		T = 323 K	
	Conc. ppm	C.R. mg.cm ⁻² .h ⁻¹	η%								
Blank	0	0.6698	--	1.808	--	2.612	--	3.573	--	4.533	--
TAC 12	5	0.1878	71.96	0.768	57.51	1.349	48.36	1.929	46.00	2.510	44.63
	10	0.1933	71.14	0.737	59.23	1.281	50.96	1.825	48.92	2.369	47.74
	20	0.1650	75.36	0.639	64.64	1.114	57.36	1.588	55.55	2.062	54.50
	30	0.1508	77.48	0.539	70.21	0.927	64.53	1.314	63.21	1.702	62.45
	40	0.1303	80.54	0.496	72.57	0.862	67.00	1.228	65.64	1.593	64.85
TBC 12	5	0.1612	75.93	0.670	62.94	1.179	54.85	1.688	52.74	2.197	51.53
	10	0.1715	74.40	0.643	64.46	1.114	57.35	1.585	55.63	2.056	54.63
	20	0.1691	74.75	0.564	68.80	0.959	63.27	1.355	62.08	1.750	61.40
	30	0.1399	79.11	0.452	74.98	0.765	70.72	1.077	69.85	1.390	69.34
	40	0.1206	82.00	0.411	77.29	0.701	73.17	0.991	72.26	1.281	71.74
	50	0.1000	85.07	0.328	81.87	0.556	78.72	0.784	78.06	1.012	77.68

3.2 Thermodynamic activation properties

The influence of temperature on the corrosion mechanism of AISI 1015 carbon steel in a 1 M HCl solution in the presence of inhibitors **TAC 12** and **TBC 12** was estimated to calculate different activation parameters. The excluded data include an analysis of activation energy (E_a^*), enthalpy of activation (ΔH^*), and entropy of activation (ΔS^*) to elucidate the thermodynamic and kinetic aspects of the corrosion process as indicated in **Table (2)**. The calculations were conducted using the Arrhenius equation **Eq. (3)** [33] and the transition state theory equation **Eq. (4)** [34].

$$\log K_{corr} = \frac{-E_a^*}{2.303 RT} + \log A \tag{3}$$

$$\log \frac{K_{corr}}{T} = \log \frac{R}{N.h} + \frac{\Delta S^*}{2.303 R} - \frac{\Delta H^*}{2.303 RT} \tag{4}$$

Where; **A** is the Arrhenius constant, **R** is the universal gas constant, **T** is the absolute temperature, **h** is the Planck's constant, and **N** is Avogadro's number. The relationship between $\log(K_{\text{corr}})$ or $\log(K_{\text{corr}}/T)$ and $(1000/T)$ is shown in **Fig. (2)**.

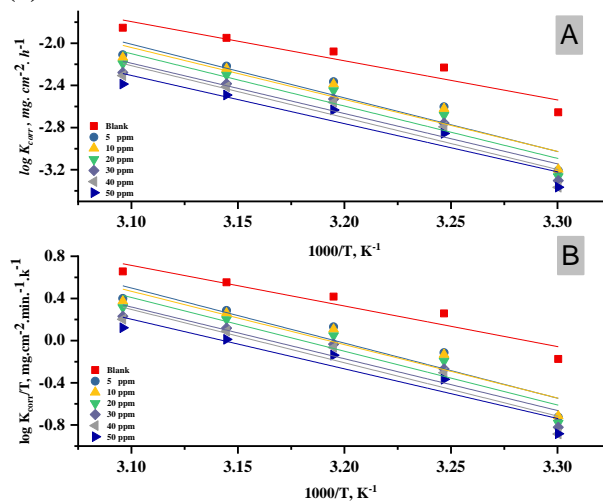


Fig (2): (A) $\log K_{\text{corr}}$ was plotted against $1000/T$ **(B)** $\log(K_{\text{corr}}/T)$ was plotted against $1000/T$, both for AISI 1015 in 1M HCL in the absence and the presence of **TAC 12** inhibitor.

The results reveal a positive value for activation energy and enthalpy, consistent with the energy barrier required for the corrosion reaction to proceed, which proves the endergonic nature of the corrosion reaction [35]. In the presence of both inhibitors, a significant increase in the activation energy of corrosion was observed, with the increase of both inhibitor concentrations [36]. The higher suggests that the inhibitor promotes the formation of a stable, protective layer on the metal surface, reducing the availability of active sites for the corrosion reaction [37]. Both chemical and physical adsorption mechanisms have been identified on steel surfaces, as evidenced by the slight increase in activation energy values between 20-80 kJ/mol [38]. Additionally, the entropy of activation indicates enhanced orderliness in the system when inhibitors are present, particularly at higher concentrations. The data extracted from activation calculation showed a similar result for both inhibitors, where **TBC 12** proved to have lower entropy when compared to **TAC 12** leading to higher adsorption onto steel surface and higher inhibition [39].

Table 2: Activation parameters of AISI 1015 carbon steel corrosion in 1M HCl without and with different inhibitor concentrations

Solution Name	Conc. ppm	E_a^* kJ/mol-1	ΔH^* kJ mol ⁻¹	ΔS^* J mol ⁻¹ K ⁻¹
Blank	0	32.0	30.9	-11.5
TAC 12	5	44.0	42.3	65.9
	10	46.1	41.0	55.8
	20	46.6	41.3	56.8
	30	47.7	39.7	43.8
	40	48.9	40.9	52.2
	50	49.1	38.0	29.5
TBC 12	5	43.8	42.6	67.0
	10	45.7	40.6	52.2
	20	48.0	38.3	34.2
	30	49.6	37.7	27.6
	40	49.0	38.7	34.6
	50	50.3	38.0	27.1

3.3 Adsorption isotherm

The corrosion inhibition mechanism of Gemini cationic surfactants **TAC 12** and **TBC 12** on AISI 1015 carbon steel surfaces was analyzed using adsorption isotherms which can be clarified by fitting experimental data to various isotherm models at various temperatures [40]. The Langmuir model shows the best fit based on the highest correlation coefficient (0.9999) [41], indicating monolayer adsorption as shown in Fig. (3). The adsorption-desorption equilibrium constant can be calculated from equation Eq. (5). The enthalpy (ΔH_{ads}°) of adsorption properties can be computed using Eq. (6) which is associated with Gibbs-Helmholtz [42]. As illustrated in Fig. (3), the adsorption-desorption equilibrium constant (K_{ads}) and enthalpy (ΔH_{ads}°) can be calculated by fitting the straight line between $\log K_{ads}$ and $1000/T$.

$$\frac{C_{inh}}{\theta} = \frac{1}{K_{ads}} + C_{inh} \quad (5)$$

$$\log K_{ads} = \frac{-\Delta H_{ads}^\circ}{2.303 RT} + \text{constant} \quad (6)$$

Where; θ is the steel's surface coverage, C_{inh} is the surfactant concentration (mol L⁻¹), K_{ads} is the adsorption equilibrium constant M⁻¹, R is the universal gas constant, and T is the temperature in kelvin. In an acidic solution, the water concentration is taken into account by factor 55.5 [43]. Both **TAC 12** and **TBC 12** inhibitors' adsorption equilibrium constants dropped, suggesting that the temperature increase reduced the amount of both inhibitors' adsorption away from the steel surface [44]. According to our analysis, the computed ΔG_{ads} values are between -20 and -40 kJ/mol, suggesting that the adsorption mechanism is mixed in nature [45]. This suggests that both chemical and physical adsorption are involved in the process. Both inhibitors spontaneously adsorb onto the steel surface, creating a protective adsorbed layer, as indicated by the negative values of ΔG_{ads} [46]. The Gibbs free energy of adsorption (ΔG_{ads}) and entropy (ΔS_{ads}°) of adsorption properties can be computed using the following equations Eq. (7) and (8) that are associated with the Gibbs-Modified Van't Hoff and Van't Hoff equations [47]. As illustrated in Fig. (3), enthalpy can be calculated by fitting the straight line between $\log K_{ads}$ and $1000/T$.

$$\Delta G_{ads} = -RT \ln 55.5 K_{ads} \tag{7}$$

$$\Delta G_{ads}^{\circ} = \Delta H_{ads}^{\circ} - T\Delta S_{ads}^{\circ} \tag{8}$$

The values of the adsorption-desorption equilibrium constant (K_{ads}), enthalpy (ΔH_{ads}°), Gibbs free energy of adsorption (ΔG_{ads}), and entropy (ΔS_{ads}°) of adsorption are summarized in **Table (3)**.

Table 3 The adsorption parameters for both inhibitors **TAC 12** and **TBC 12** on steel surfaces at different temperature

Surfactant name	Temp K	K_{ads} M ⁻¹	ΔG_{ads}° kJ mol ⁻¹	ΔH_{ads}° kJ mol ⁻¹	ΔS_{ads}° J mol ⁻¹ K ⁻¹
TAC 12	303	592.4	-26.2	-57.9	-104.6
	308	241.5	-24.3		-108.9
	313	157.7	-23.6		-109.5
	318	141.4	-23.7		-107.5
	323	132.8	-23.9		-105.2
TBC 12	303	478.5	-25.7	-41.7	-52.92
	308	268.1	-24.6		-55.51
	313	189.4	-24.1		-56.23
	318	174.5	-24.3		-54.82
	323	166.4	-24.5		-53.19

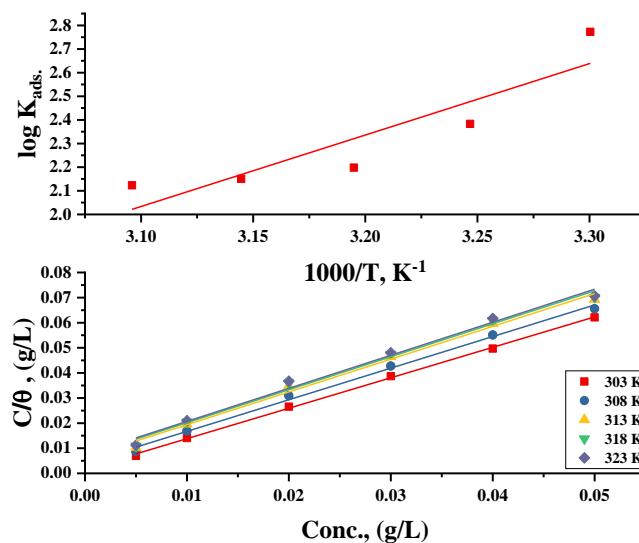


Fig (3): Langmuir adsorption isotherm model, C/θ vs C for AISI 1015 carbon steel with different concentrations (5 to 50 ppm) of TAC 12 at different temperatures

The adsorption process becomes exothermic [48] when the negative enthalpy for both **TAC 12** and **TBC 12** inhibitors is indicated to be -57.9 and -41.7 kJ/mol respectively, indicating mixed interactions between the inhibitor molecules and the steel surface, including physical and chemical adsorption [49]. The adsorption process is physisorption when the value is less than -40 kJ mol⁻¹ and chemisorption when the value is greater than -100 kJ mol⁻¹. An increase in the negative entropy values for **TAC 12** and **TBC 12** cationic Gemini surfactants indicates that the adsorption process is becoming more rigid, which decreases again at higher temperatures 313-323 K, indicating a feature of the mixed adsorption mechanism that combines physical and chemical adsorption [50-51]. This could be explained by the

transition from a less ordered adsorption layer to a more structured one as the inhibitor concentration increases [52].

3.4 Potentiodynamic polarization test

A potentiodynamic polarization test was used to investigate the corrosion behavior of steel specimens in a 1 M hydrochloric acid solution, both with and without varying inhibitor concentrations which are shown in **Fig. (4)** and **(5)**. The extrapolated linear regions of the Tafel plots were used to indicate the polarization parameters, which include corrosion potential (E_{corr}), corrosion current density (I_{corr}), anodic Tafel slope (β_a), and cathodic Tafel slope (β_c) which are summarized in **Table 4**. Additionally, displays the inhibition efficiencies ($IE\%$) and surface coverage (θ), that can be computed by using **Eq. (9)**.

$$IE \% = \theta \times 100 = \left[1 - \frac{I_{inh.}}{I_b} \right] \times 100 \tag{9}$$

The corrosion current densities of inhibited and uninhibited solutions are denoted by $I_{inh.}$ and I_b , respectively. One important criterion for determining the type of corrosion inhibitor action is the change in corrosion potential. An anodic or cathodic inhibitor is usually indicated by a displacement larger than 85 mV, either in the positive or negative direction [53]. Both inhibitors indicated a decrease in the corrosion reaction in both anodic and cathodic reactions with a dominant displacement toward the cathodic side (β_c) for both tested inhibitors, **TAC 12** and **TBC 12**, which is greater than 85 mV [54]. Accordingly, the inhibitors are classified as primarily cathodic, demonstrating their important role in inhibiting the cathodic reaction, especially the evolution of hydrogen gas [55]. The corrosion inhibition efficiencies in the presence of both inhibitors were increased with increasing concentration. While **TBC 12** confirmed more inhibition through adsorbing more on steel surfaces especially at low concentrations compared to **TAC 12** [56].

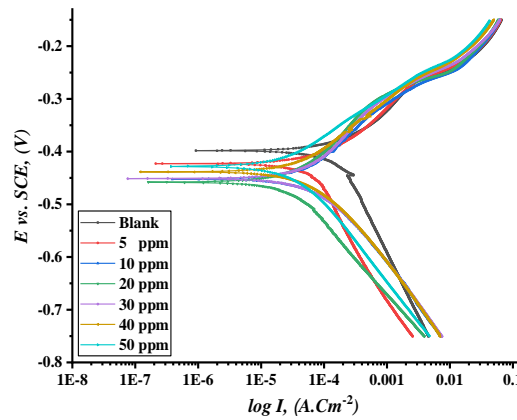


Fig (4): Potentiodynamic polarization curves ($\log I$ plotted against $E vs. SCE$) of AISI 1015 carbon steel in 1M HCl without and with different concentrations of inhibitor (TAC 12)

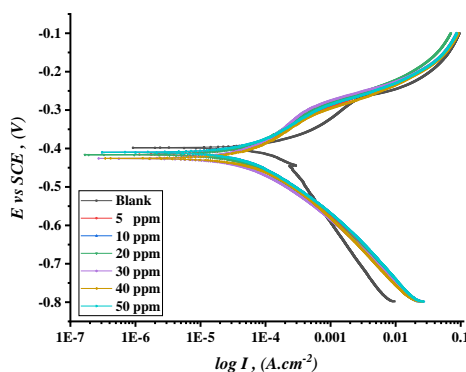


Fig (5): Potentiodynamic polarization curves ($\log I$ plotted against E vs. SCE) of AISI 1015 carbon steel in 1M HCl without and with different concentrations of inhibitor (TBC 12)

Table 4 potentiodynamic polarization parameters for both TAC 12 and TBC 12 inhibitors in 1M HCl solution at 303 K.

Surf. Name	Conc. ppm	I_{corr} $\mu A\ Cm^{-2}$	$-E_{corr}$ mV	β_a mV/dec	β_c mV/dec	% η	θ
Blank	0.0	287	389.00	145.0	381.0	--	--
TAC 12	5	160	423.00	120.9	144.9	44.25	0.443
	10	72	452.00	150.0	126.3	75.09	0.751
	20	54	458.00	137.4	183.5	81.18	0.812
	30	58	451.00	138.8	117.2	79.69	0.797
	40	50	438.00	117.2	125.6	82.68	0.827
	50	42	428.00	97.00	148.0	85.37	0.854
TBC 12	5	53	410.00	100.2	122.2	81.39	0.814
	10	53	384.00	89.20	338.8	81.53	0.815
	20	50	416.00	119.5	130.3	82.58	0.826
	30	48	426.00	141.4	123.1	83.28	0.833
	40	47	407.00	78.30	145.0	83.62	0.836
	50	40	401.00	74.10	157.9	86.06	0.861

3.5 Electrochemical impedance spectroscopy (EIS)

The electrochemical impedance spectroscopy analysis was performed to assess the corrosion inhibition efficiency of TAC 12 and TBC 12 cationic Gemini surfactants on AISI 1015 carbon steel in a 1 M hydrochloric acid solution. A modified constant phase element equivalent circuit was used to model the impedance response, incorporating electrolyte resistance (R_s), pores constant phase element (CPE_f), constant phase element (CPE_{dl}), interface resistance (R_{po}), and charge transfer resistance (R_{ct}), as illustrated in Fig. (6) [57]. The results, summarized in Table 5, reveal key trends in the performance of both inhibitors.

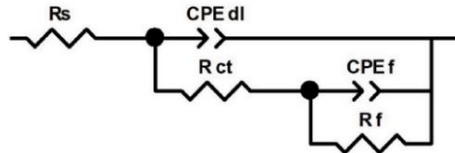


Figure 6: The modified equivalent circuit used in fitting the corrosion inhibition mechanism of both inhibitors on an AISI 1015 carbon steel surface.

The presence of inhibitors led to a significant increase in charge transfer resistance compared to the uninhibited solution, confirming enhanced resistance to electron transfer at the steel-electrolyte interface [58]. Additionally, the capacitive loop diameter increased with higher inhibitor concentrations, as shown in Fig. (7), indicating the formation of a protective inhibitor layer on the steel surface [59]. The decrease in double-layer capacitance with increasing inhibitor concentration further supports this observation, as it suggests a reduction in the active surface area exposed to the corrosive medium, reinforcing the adsorption effectiveness of the inhibitors [60].

The degree of surface heterogeneity varied with inhibitor adsorption, with TBC 12 forming a more uniform protective layer compared to TAC 12 [61]. The analysis of pore resistance (R_{po}) revealed that TAC 12 resulted in higher values, indicating the formation of pores in the inhibitor layer over time due to water and chloride ion penetration [62]. These conductive pores, filled with the aggressive electrolyte, led to an increase in pores resistance [63]. The pore resistance of TAC 12 decreased with increasing concentrations of inhibitor due to providing greater surface coverage. In contrast, TBC 12 formed a denser and more dielectric protective layer, as evidenced by its negligible pore resistance values, suggesting no electrolyte penetration [64].

$$IE \% = \theta \times 100 = \left[1 - \frac{R_{ct}^0}{R_{ct}} \right] \times 100 \tag{10}$$

The inhibition efficiency (IE%) and surface coverage (θ) values, calculated from the impedance data using the relevant equation Eq. (10), confirmed the effectiveness of both inhibitors in mitigating corrosion. The Bode plots, presented in Fig. (8), demonstrate that impedance decreases with increasing frequency across all tested concentrations, consistent with the behavior of well-adsorbed protective layers [65]. Overall, the findings indicate that TBC 12 provides superior corrosion protection due to its more compact and homogeneous inhibitor film, whereas TAC 12, despite offering significant inhibition, exhibits increased porosity over time.

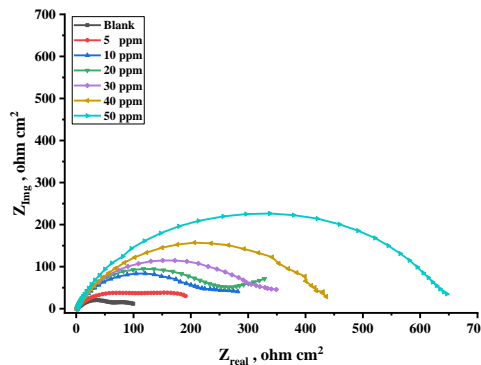
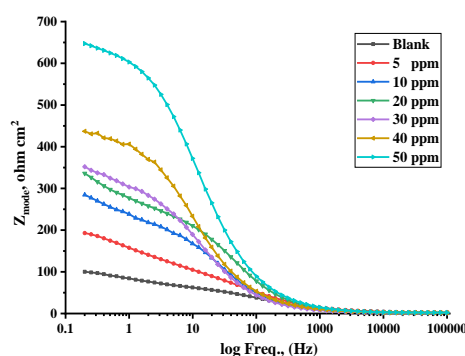


Fig (7): EIS Nyquist of AISI 1015 carbon steel in 1M HCl without and with different concentrations of inhibitor (TAC 12)



Fig(8): EIS Bode of AISI 1015 carbon steel in 1M HCl without and with different concentrations of inhibitor (TAC 12)

Table 5 EIS parameter values of AISI 1015 carbon steel corrosion in 1M HCl without and with different concentrations of all Gemini cationic surfactants at 303 K

	conc. (ppm)	R_s $\Omega.cm^2$	R_{ct} Ωcm^2	CPE $\mu F cm^{-2}$	n_1	C_c $\mu F cm^{-2}$	R_{Po} $\Omega.cm^2$	n_2	IE %	Θ
Blank	0	1.73	83	8071	0.130	10700	--	0.120	--	--
TAC 12	5	1.80	197	4980	0.123	111.0	6.85E-04	0.750	58.33	0.853
	10	1.77	335	1246	0.112	111.0	6.85E-06	0.740	75.52	0.755
	20	1.50	448	223	0.098	104.0	1.16E-07	0.780	81.68	0.817
	30	1.50	464	545	0.083	90.00	1.60E-06	0.820	82.32	0.823
	40	1.88	500	248	0.104	47.00	2.60E-08	0.790	83.60	0.836
	50	2.04	639	456	0.101	8.000	1.10E-09	0.840	87.17	0.872
TBC 12	5	1.62	286.60	173.0	0.786	3.000	0	0.000	71.39	0.71
	10	1.70	407.00	183.0	0.791	2.500	0	0.020	79.85	0.80
	20	2.07	504.00	180.0	0.784	2.500	0	0.030	83.73	0.84
	30	1.70	522.00	173.0	0.782	2.500	0	0.050	84.29	0.84
	40	1.60	530.00	137.0	0.819	3.200	0	0.060	84.53	0.85
	50	1.60	755.00	142.0	0.806	2.700	0	0.080	89.14	0.89

3.6 Computations for Quantum Chemistry

Quantum simulations using Gaussian 9.0 examined the effect of molecular structure on inhibition efficiency through complete geometry optimization with the B3LYP functional and 6-31G (d,p) basis set. Key quantum chemical parameters were derived from HOMO and LUMO energies. These calculations provided insights into the electronic properties influencing inhibitor performance as shown in **Eq. (11-16)**.

$$\text{Ionization potential } (I) = -E_{HOMO} \quad (11)$$

$$\text{Electron affinity } (A) = -E_{LUMO} \quad (12)$$

$$\text{Electronegativity } (\chi) = \frac{I + A}{2} \quad (13)$$

$$\text{Global hardness } (\eta) = \frac{I - A}{2} \quad (14)$$

$$\text{Softness } (\sigma) = \frac{1}{\eta} \quad (15)$$

$$\text{Electron transfer fraction } (\Delta N) = \frac{(\chi_{\text{Fe}} - \eta_{\text{Inh}})}{2(\eta_{\text{Fe}} + \eta_{\text{Inh}})} \quad (16)$$

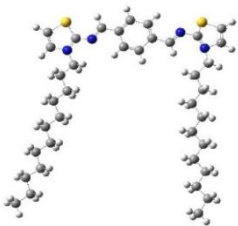
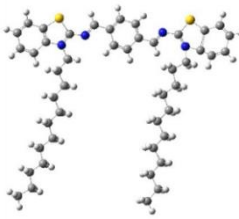
A quantum chemical analysis was conducted to examine the electronic properties and molecular structures of **TAC 12** and **TBC 12**, with a focus on their role in corrosion inhibition and correlation with experimental findings from gravimetric and electrochemical studies [66]. The analysis of frontier molecular orbitals revealed that both inhibitors exhibit high electron-donating potential, as indicated by their elevated highest occupied molecular orbital (HOMO) energy levels, while their low lowest unoccupied molecular orbital (LUMO) energies suggest a strong ability to accept electrons.

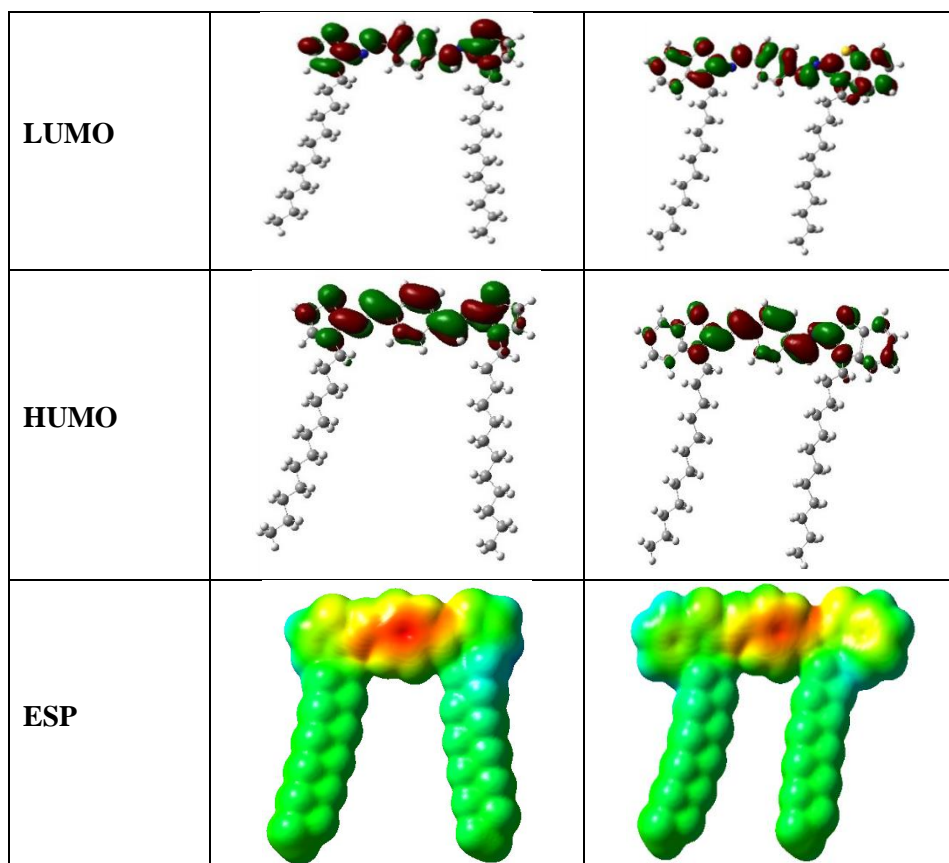
Comparative evaluation of the two inhibitors demonstrated that **TBC 12** possesses a higher HOMO energy (-2.7067 eV) and lower LUMO energy (-1.6885 eV) than **TAC 12** (-2.1655 eV and -1.1247 eV, respectively), which can be attributed to the presence of additional aromatic rings while maintaining the same heteroatoms, such as sulfur and nitrogen [67]. This structural difference enhances the adsorption efficiency of **TBC 12** on the metal surface, as illustrated in **Table 6**. The lower energy gap observed for **TBC 12** (1.0183 eV) compared to **TAC 12** (1.0408 eV) further supports its superior reactivity and adsorption capability [68]. The electronic softness and hardness values reinforce this trend, with the **TBC 12** inhibitor displaying higher softness (1.9642) and lower hardness (0.5091) compared to **TAC 12** (1.9215) and (0.5204) respectively, indicating a more favorable interaction with the metal surface and improved inhibition performance [69].

The fraction of electron transfer (ΔN), which measures the electron-donating capacity of the inhibitors, was found to be higher for **TAC 12** (5.1449) than **TBC 12** (4.7163), demonstrating its enhanced ability to transfer electrons to the metal [70]. While **TBC 12** may offer better surface coverage due to bigger molecular size, planarity, or hydrophobic interactions, leading to more surface coverage and improved inhibition [71]. **TBC 12** has a higher electronegativity (2.1976), and it has a stronger tendency to attract electrons, which may contribute to its better adsorption efficiency and corrosion inhibition performance compared to **TAC 12** (1.6451) [72].

These quantum chemical findings validate the experimental results, confirming that **TBC 12** exhibits superior adsorption and corrosion inhibition efficiency compared to **TAC 12**. The theoretical predictions align with the observed electrochemical and gravimetric data, as summarized in **Table 6**, reinforcing the role of molecular structure in determining inhibition effectiveness.

Table 6 Calculated parameters for the TAC 12 and TBC 12 series inhibitors obtained using the DFT method at the B3LYP/6-31G(d,p) basis set.

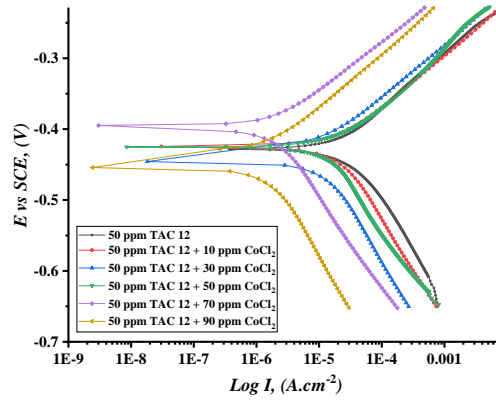
Name	TAC 12	TBC 12
Structure		



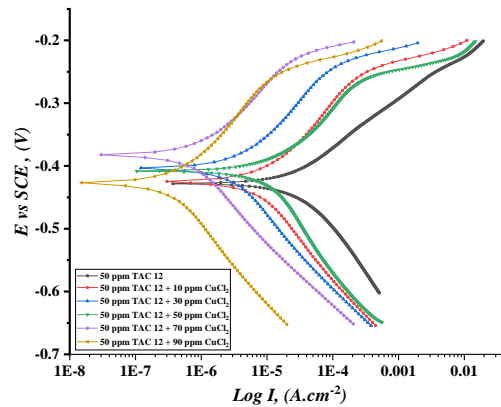
3.7 Synergism of corrosion inhibition under the influence of salts

3.7.1 Potentiodynamic polarization tests

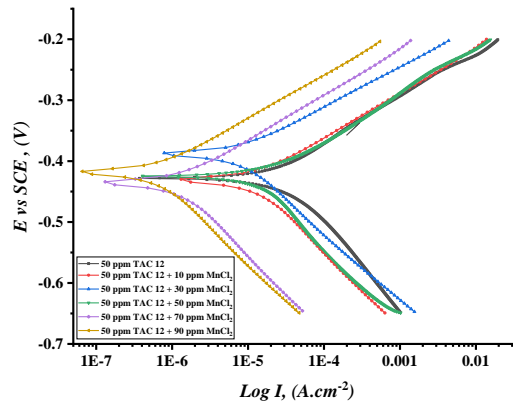
The synergistic effect of Gemini cationic surfactants in conjunction with inorganic salts (CoCl_2 , MnCl_2 , and CuCl_2) on steel corrosion inhibition was analyzed through polarization measurements **Fig. (9-11)**. The polarization parameters, including corrosion potential (E_{corr}), current density (I_{corr}), and anodic and cathodic Tafel slopes (β_a , β_c), are presented in **Table 7**. The addition of salts resulted in a notable shift in both anodic and cathodic curves towards lower current density, following the trend $\text{CuCl}_2 > \text{MnCl}_2 > \text{CoCl}_2$, which indicates an enhancement in inhibition efficiency [73]. This improvement can be attributed to synergistic adsorption, wherein chloride anions from the salts initially chemisorb onto the steel surface [74], forming an active layer that facilitates the subsequent adsorption of inhibitor molecules [75]. The cationic surfactant components are then adsorbed through electrostatic interactions, leading to the formation of a protective film that significantly increases surface coverage and corrosion resistance [76]. The moderate shift in (E_{corr}) suggests that the inhibitors function as mixed-type corrosion inhibitors, reducing both anodic metal dissolution and cathodic hydrogen evolution [77]. The effectiveness of the inhibitors follows the order $\text{CuCl}_2 > \text{MnCl}_2 > \text{CoCl}_2$, which can be explained by the physicochemical properties of the metal ions. Cu^{2+} ions, possessing a higher charge density and smaller ionic radius [78], exhibit stronger interactions with the inhibitor molecules, resulting in the formation of a more compact and stable protective layer compared to Mn^{2+} and Co^{2+} [79]. Additional factors, including salt solubility, modifications in the electrical double layer, and coordination chemistry, further contribute to this trend, with CuCl_2 demonstrating the most substantial corrosion protection [80].



Fig(9): Potentiodynamic polarization curves (log I plotted against E vs. SCE) of AISI 1015 carbon steel in 1M HCl for TAC 12 surfactant at 50 ppm with the addition of different concentrations of CoCl₂



Fig(10): Potentiodynamic polarization curves (log I plotted against E vs. SCE) of AISI 1015 carbon steel in 1M HCl for TAC 12 surfactant at 50 ppm with the addition of different concentrations of CuCl₂



Fig(11): Potentiodynamic polarization curves (log I plotted against E vs. SCE) of AISI 1015 carbon steel in 1M HCl for TAC 12 surfactant at 50 ppm with the addition of different concentrations of MnCl₂

Table 7 Data from PDP test for corrosion of AISI 1015 carbon steel in 1M HCl at 50 ppm of both cationic Gemini surfactants in the presence of different salt concentrations at 303K

Surf. Name	Salt name	Salt conc. ppm	I_{corr} $\mu\text{A Cm}^{-2}$	$-E_{corr}$ mV	β_a mV/dec	β_c mV/dec	$\% \eta$	θ	
TAC 12	No salt	0	42.00	428	97.0	148.0	85.37	0.854	
	CoCl₂	10	28.29	425	73.3	151.9	90.14	0.901	
		30	26.10	446	73.8	156.9	90.91	0.909	
		50	23.74	426	79.5	133.3	91.73	0.917	
		70	20.97	393	73.9	133.9	92.69	0.927	
		90	20.79	455	74.9	158.3	92.76	0.928	
	CuCl₂	10	16.96	426	73.9	130.0	94.09	0.941	
		30	14.58	401	66.5	120.0	94.92	0.949	
		50	16.20	408	81.8	129.3	94.36	0.944	
		70	10.77	385	62.8	110.0	96.25	0.962	
		90	8.88	427	59.1	110.0	96.91	0.969	
	MnCl₂	10	18.30	433	70.0	144.7	93.62	0.936	
		30	14.87	386	70.0	156.9	94.82	0.948	
		50	16.98	425	89.2	117.3	94.08	0.941	
		70	15.00	435	70.0	164.3	94.77	0.948	
		90	13.94	419	70.0	171.8	95.14	0.951	
	TBC 12	No salt	0	40.00	401	74.1	157.9	86.06	0.861
		CoCl₂	10	25.43	446	88.7	101.7	91.14	0.911
			30	24.04	463	82.0	111.7	91.62	0.916
			50	22.52	412	67.0	153.3	92.15	0.922
70			21.69	430	87.8	113.0	92.44	0.924	
90			20.19	449	87.5	119.6	92.97	0.930	
CuCl₂		10	16.75	431	60.00	290.0	94.16	0.942	
		30	12.35	388	60.00	113.0	95.70	0.957	
		50	21.59	387	108.6	223.0	92.48	0.925	
		70	9.17	365	50.00	107.2	96.80	0.968	
		90	8.25	344	50.00	100.9	97.13	0.971	
MnCl₂		10	17.65	429	61.90	138.3	93.85	0.939	
		30	16.05	387	55.70	124.5	94.41	0.944	
		50	15.44	412	52.60	117.6	94.62	0.946	
		70	14.53	367	49.50	110.0	94.94	0.949	
		90	11.87	344	46.40	103.7	95.86	0.959	

3.7.2 Electrochemical impedance spectroscopy test

The synergistic inhibition of steel corrosion in 1 M HCl was investigated in the presence of CoCl₂, MnCl₂, and CuCl₂, revealing a significant enhancement in inhibition efficiency when combined with TAC 12 and TBC 12 cationic Gemini surfactants. Electrochemical impedance spectroscopy (EIS) data were analyzed using various equivalent circuits, with Randall's circuit providing the best fit, as illustrated in Fig. (12) [81].

Nyquist plots Fig. (13-15) demonstrated an increase in semicircle diameter with rising salt concentrations, indicating improved corrosion resistance [82]. Among the salts studied, CuCl₂ exhibited the largest semicircle diameter, signifying the highest inhibition efficiency, followed by MnCl₂ and CoCl₂. This trend was further corroborated by an increase in polarization resistance (R_p) and a concurrent

decrease in constant phase element (CPE) values, confirming the formation of a stable and protective inhibitor layer, particularly in the presence of CuCl_2 [83]. The Bode curves shown in Fig. (16-18) reinforced these observations, with CuCl_2 displaying the most pronounced enhancement in impedance magnitude and phase angle, indicative of superior corrosion resistance [84].

The increase in impedance magnitude with higher salt concentrations reflects improved surface protection, with CuCl_2 forming the most stable and adherent inhibitor layer compared to MnCl_2 and CoCl_2 . These findings, summarized in Table 8, underscore the superior corrosion inhibition efficiency of CuCl_2 due to its ability to facilitate stronger interactions with inhibitor molecules, leading to the formation of a more compact and protective surface film [85].

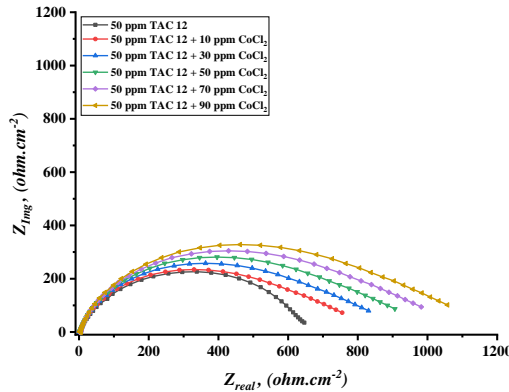
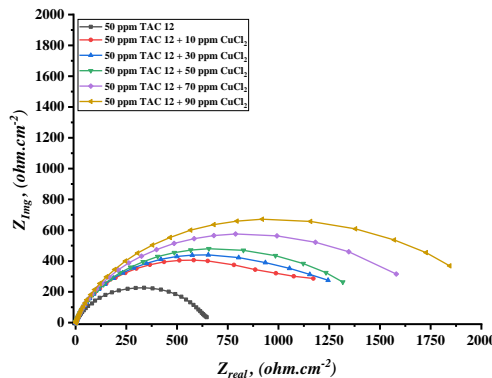
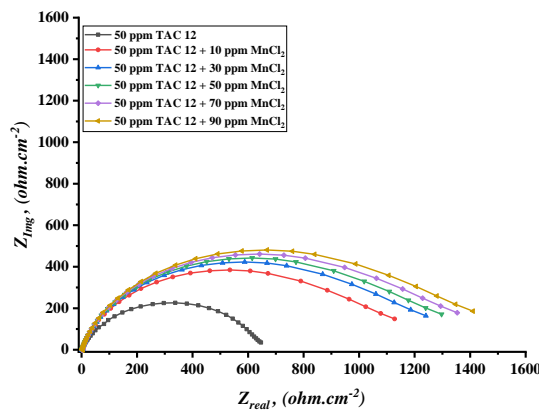


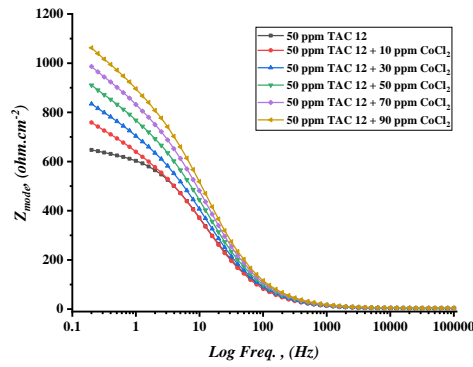
Fig (13): *EIS Nyquist* of AISI 1015 carbon steel in 1M HCl with the highest concentration of inhibitor (TAC 12) in the presence of different concentrations of CoCl_2 salt



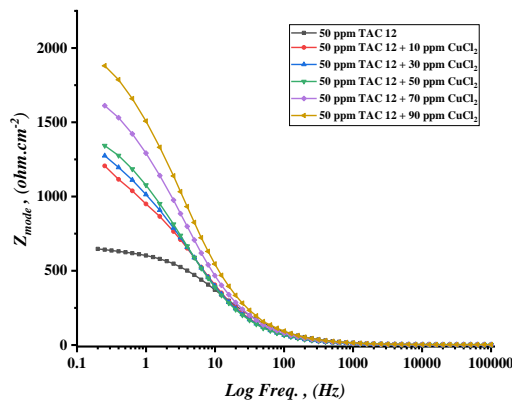
Fig(14): *EIS Nyquist* of AISI 1015 carbon steel in 1M HCl with the highest concentration of inhibitor (TAC 12) in the presence of different concentrations of CuCl_2 salt



Fig(15): *EIS Nyquist* of AISI 1015 carbon steel in 1M HCl with the highest concentration of inhibitor (TAC 12) in the presence of different concentrations of MnCl_2 salt



Fig(16): *EIS Bode* of AISI 1015 carbon steel in 1M HCl at 50 ppm of inhibitor (TAC 12) with the addition of different concentrations of CoCl_2 salt



Fig(17): *EIS Bode* of AISI 1015 carbon steel in 1M HCl at 50 ppm of inhibitor (TAC 12) with the addition of different concentrations of CuCl_2 salt

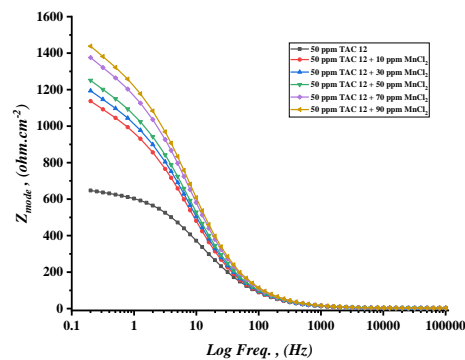


Fig (18): *EIS Bode* of AISI 1015 carbon steel in 1M HCl at 50 ppm of inhibitor (TAC 12) with the addition of different concentrations of MnCl_2 salt

Table 8 Data from PP test for corrosion of AISI 1015 carbon steel in 1M HCl at 50 ppm of different Gemini cationic surfactants in the presence of different concentrations of CoCl₂ salt at 303K

Surf. name	Salt name	Salt conc. ppm	R_p $\Omega.cm^2$	CPE $\mu F cm^{-2}$	IE %	θ
TAC 12	No salt	0	639	0.0000456	87.17	0.872
	CoCl ₂	10	759	0.0000241	90.45	0.905
		30	835	0.0000232	90.84	0.908
		50	911	0.0000223	91.00	0.910
		70	986	0.0000142	91.96	0.920
		90	1062	0.0000020	93.50	0.935
	CuCl ₂	10	1206	0.0000045	93.20	0.932
		30	1274	0.0000040	93.56	0.936
		50	1343	0.0000031	94.32	0.943
		70	1612	0.0000028	95.21	0.952
		90	1880	0.0000027	95.86	0.959
	MnCl ₂	10	1137	0.0000029	92.79	0.928
		30	1194	0.0000023	93.66	0.937
		50	1251	0.0000020	93.93	0.939
		70	1376	0.0000019	94.04	0.940
		90	1438	0.0000018	94.30	0.943
	TBC 12	No salt	0	755	0.0000030	89.14
CoCl ₂		10	809	0.0000098	91.47	0.915
		30	854	0.0000074	91.92	0.919
		50	899	0.0000056	92.32	0.923
		70	989	0.0000031	93.02	0.930
		90	1087	0.0000024	93.65	0.937
CuCl ₂		10	1289	0.0000064	94.65	0.947
		30	1378	0.0000041	94.99	0.950
		50	1469	0.0000029	95.30	0.953
		70	1614	0.0000023	95.72	0.957
		90	1760	0.0000021	96.08	0.961
MnCl ₂		10	886	0.0000096	92.21	0.922
		30	978	0.0000067	92.94	0.929
		50	1070	0.0000030	93.55	0.936
		70	1177	0.0000026	94.14	0.941
		90	1287	0.0000021	94.64	0.946

3.8 Mechanism of inhibition

The inhibition mechanism of Gemini cationic surfactants is governed by the formation of a protective film on the steel surface, following the Langmuir adsorption isotherm. Adsorption occurs through a mixed physisorption and chemisorption process, where electrostatic interactions between the positively charged quaternary ammonium groups and the negatively charged steel surface facilitate physical adsorption, aided by the presence of bromide (Br⁻) and chloride (Cl⁻) ions. Concurrently, chemical adsorption occurs via covalent bonding and donor-acceptor interactions involving heteroatoms and aromatic rings, leading to the stabilization of the protective layer and a reduction in the hydrogen evolution reaction at cathodic sites. The **TAC 12** inhibitor forms a protective film that, over time, transfers porosity, allowing corrosive chloride ions to penetrate and compromise its integrity, resulting in a conductive and less effective barrier. In contrast, **TBC 12** inhibitor establishes a denser, non-porous, and insulating layer, offering superior corrosion resistance. Experimental and theoretical analyses confirmed that TBC 18 exhibits higher surface coverage and inhibition efficiency than TBC 6, demonstrating the impact of molecular structure on performance. The addition of CoCl₂, MnCl₂, and CuCl₂ alters the inhibition mechanism from predominantly cathodic to a mixed-type inhibition. The

cooperative adsorption of chloride ions from these salts generates a negatively charged layer on the steel surface, enhancing the attraction of cationic surfactant molecules. Simultaneously, metal cations (Mn^{2+} , Co^{2+} , Cu^{2+}) interact with both the surfactant and the steel surface, reinforcing the protective film and improving its ability to inhibit both hydrogen evolution and iron dissolution. This synergistic effect significantly enhances corrosion resistance, particularly in the presence of Cu^{2+} ions, which form a more stable and compact inhibitor layer.

4. CONCLUSION

This study demonstrates the efficacy of cationic Gemini surfactants with distinct structural head groups—thiazole (TAC 12) and benzo[d]thiazole (TBC 12)—as corrosion inhibitors for steel in 1M HCl solution. Experimental and theoretical analyses confirm the formation of a protective adsorption film that follows the Langmuir adsorption isotherm. Gravimetric weight loss measurements indicate high inhibition efficiencies, reaching 85% for TBC 12 and 80% for TAC 12. However, inhibition efficiency declines with increasing temperature, correlating with reduced surface coverage. Activation and adsorption parameters confirm a mixed adsorption mechanism, influencing both iron dissolution and hydrogen evolution reactions, with a predominant cathodic control. Distinct inhibition behaviors were observed: TAC 12 formed a porous, conductive film, allowing penetration of the corrosive medium, whereas TBC 12 created a dense, non-porous insulating layer, offering superior corrosion protection. The incorporation of inorganic salts ($CoCl_2$, $MnCl_2$, $CuCl_2$) enhanced inhibition efficiency by stabilizing the protective film and shifting the inhibitors' behavior towards a mixed-type inhibition mechanism.

5. Acknowledgment

“Not applicable” in this section.

6. Conflict of interest

There is no conflict of interest.

7. Fund

This study was carried out without any type of funds

8. Data availability

Raw data were generated at Faculty of Science, Port-Said University, Egypt. Derived data supporting the findings of this study are available from the corresponding author, Prof. Dr. Samir A. Abd El-Maksoud, on request.

9. Authors contribution

- **Samir A. Abd El-Maksoud:** Participated in writing the scientific material for the linguistic revision manuscript.
- **Mohamed A. Migahed:** Participated in writing the scientific material for the linguistic revision manuscript.
- **Mahmoud M. Gouda:** Participate in writing the scientific material for the manuscript and conducting the practical aspect.
- **Farid I. El-Dossoki:** Participated in writing the scientific material for the linguistic revision manuscript.

10. REFERENCES

- [1] T. Islam and H. M. M. A. Rashed, "Classification and Application of Plain Carbon Steels," *Ref. Modul. Mater. Sci. Mater. Eng.*, 2019, doi: 10.1016/B978-0-12-803581-8.10268-1.
- [2] M. Y. Demeri, "Mechanical Working (Strain Hardening)," *Adv. High-Strength Steels - Sci. Technol. Appl.*, 2013, Accessed: Jan. 21, 2025.
- [3] X. Yi, C. Yong-kang, T. Jing-lei, S. Wei, W. Wei-li, Z. Xi, L. Yi, Z. Xiu-juan, X. Yi, C. Yong-kang, T. Jing-lei, S. Wei, W. Wei-li, Z. Xi, L. Yi, and Z. Xiu-juan, "Application status and prospect of low carbon technology in iron and steel industry," *Chinese J. Eng. 2022, Vol. 44, Issue 4, Pages 801-811*, vol. 44, no. 4, pp. 801–811, Apr. 2022, doi: 10.13374/J.ISSN2095-9389.2021.08.01.001.
- [4] D. Kumar, J. M. Khan, M. Posa, A. K. Pulikkal, B. Saha, and A. Bhattacharai, "Effect of Quaternary Ammonium Gemini Surfactant Solution on the Rate Constant of the Ninhydrin-Lysine Reaction," *Ind. Eng. Chem. Res.*, vol. 62, no. 39, pp. 15897–15906, Oct. 2023, doi: 10.1021/ACS.IECR.3C02499/SUPPL_FILE/IE3C02499_SI_001.PDF.
- [5] H. S. Aljibori, A. Alamiery, and A. A. H. Kadhum, "Advances in corrosion protection coatings: A comprehensive review," *Int. J. Corros. Scale Inhib.*, vol. 12, no. 4, pp. 1476–1520, 2023, doi: 10.17675/2305-6894-2023-12-4-6.
- [6] S. Kumari, S. Chauhan, A. Umar, H. Fouad, and M. S. Akhtar, "Conductometric and Fluorescence Probe Analysis to Investigate the Interaction between Bioactive Peptide and Bile Salts: A Micellar State Study," *Molecules*, vol. 27, no. 21, p. 7561, Nov. 2022, doi: 10.3390/MOLECULES27217561/S1.
- [7] H. Aljibori, A. Al-Amiery, and W. N. R. Isahak, "Advancements in Corrosion Prevention Techniques," *J. Bio- Tribo-Corrosion*, vol. 10, no. 4, pp. 1–31, Dec. 2024, doi: 10.1007/S40735-024-00882-W/METRICS.
- [8] G. Koch, "Cost of corrosion," *Trends Oil Gas Corros. Res. Technol. Prod. Transm.*, pp. 3–30, Jan. 2017, doi: 10.1016/B978-0-08-101105-8.00001-2.
- [9] A. Al-Amiery, W. N. R. Wan Isahak, and W. K. Al-Azzawi, "Sustainable corrosion Inhibitors: A key step towards environmentally responsible corrosion control," *Ain Shams Eng. J.*, vol. 15, no. 5, p. 102672, May 2024, doi: 10.1016/J.ASEJ.2024.102672.
- [10] B. Brycki and A. Szulc, "Gemini surfactants as corrosion inhibitors. A review," *J. Mol. Liq.*, vol. 344, p. 117686, Dec. 2021, doi: 10.1016/J.MOLLIQ.2021.117686.
- [11] G. Wei, S. Deng, D. Shao, D. Xu, R. Lei, and X. Li, "Gemini cationic surfactant of 1, 3-bis (dodecyl dimethyl ammonium chloride) propane as a novel excellent inhibitor for the corrosion of cold rolled steel in HCl solution," *J. Colloid Interface Sci.*, vol. 677, pp. 324–345, Jan. 2025, doi: 10.1016/J.JCIS.2024.07.229.
- [12] C. Wang and E. Yang, "Experimental and computational studies of cationic Gemini surfactants as corrosion inhibitors for carbon steel in 15% HCl," *Phys. Chem. Chem. Phys.*, 2024, doi: 10.1039/D4CP03616F.
- [13] L. Liu, C. Wang, J. Du, Y. Zuo, L. Zhang, X. Hu, and Z. Xu, "Adsorption of cationic Gemini surfactants on carbon steel surface and their anticorrosion performance in hydrochloric acid solution," *J. Surfactants Deterg.*, Jan. 2025, doi: 10.1002/JSDE.12831.
- [14] H. Chen, Y. Zhang, L. Xiao, and L. Hou, "Synthesis of Schiff-base cationic Gemini surfactant and the properties for inhibiting corrosion of Q235 carbon steel and printed circuit board," *J. Surfactants Deterg.*, vol. 27, no. 2, pp. 197–210, Mar. 2024, doi: 10.1002/JSDE.12716.
- [15] Y. Xiong and M. Cao, "Application of surfactants in corrosion inhibition of metals," *Curr. Opin. Colloid Interface Sci.*, vol. 73, p. 101830, Oct. 2024, doi: 10.1016/J.COCIS.2024.101830.
- [16] Y. A. Selim, M. Abd-El-Raouf, K. Zakaria, A. Z. Sayed, Y. M. Moustafa, and A. M. Ashmawy,

- “An electrochemical, and surface studies of synthesized Gemini ionic liquid as corrosion inhibitor for carbon steel in petroleum field,” *Sci. Reports 2024 141*, vol. 14, no. 1, pp. 1–16, May 2024, doi: 10.1038/s41598-024-58321-2.
- [17] M. En-Nyly, S. Skal, Y. El Aoufir, H. Serrar, H. Lgaz, S. Boukhris, O. Benali, T. Guedira, and H. seung Lee, “Elucidating the mechanisms of novel thiazole-based corrosion inhibitors in carbon steel/HCl interface: An integrated approach combining experimental and computational studies,” *J. Mol. Struct.*, vol. 1306, p. 137817, Jun. 2024, doi: 10.1016/J.MOLSTRUC.2024.137817.
- [18] R. A. Omer, P. Koparir, and L. O. Ahmed, “Characterization and Inhibitor Activity of Two Newly Synthesized Thiazole,” *J. Bio- Tribo-Corrosion*, vol. 8, no. 1, pp. 1–12, Mar. 2022, doi: 10.1007/S40735-021-00625-1/FIGURES/6.
- [19] Z. Liu, B. Fan, J. Zhao, B. Yang, and X. Zheng, “Benzothiazole derivatives-based supramolecular assemblies as efficient corrosion inhibitors for copper in artificial seawater: Formation, interfacial release and protective mechanisms,” *Corros. Sci.*, vol. 212, p. 110957, Mar. 2023, doi: 10.1016/J.CORSCI.2022.110957.
- [20] L. Cui, Y. Lv, Y. Dong, H. Liao, S. Wu, and X. Li, “Benzothiazole-based ionic liquids as environment-friendly and high-efficiency corrosion inhibitors for mild steel in HCl: Experimental and theoretical studies,” *J. Mol. Liq.*, vol. 394, p. 123769, Jan. 2024, doi: 10.1016/J.MOLLIQ.2023.123769.
- [21] C. Verma, A. Thakur, R. Ganjoo, S. Sharma, H. Assad, A. Kumar, M. A. Quraishi, and A. Alfantazi, “Coordination bonding and corrosion inhibition potential of nitrogen-rich heterocycles: Azoles and triazines as specific examples,” *Coord. Chem. Rev.*, vol. 488, p. 215177, Aug. 2023, doi: 10.1016/J.CCR.2023.215177.
- [22] S. Shadi, G. Bahlakeh, B. Ramezanzadeh, and A. H. J. Mofidabadi, “Experimental and computational exploration of synergistic effect of Laurus nobilis extract:Zinc cation on mild steel corrosion inhibition in saline solution,” *J. Mol. Liq.*, vol. 385, p. 122424, Sep. 2023, doi: 10.1016/J.MOLLIQ.2023.122424.
- [23] Y. Zhang, X. Niu, J. Zhou, J. Wang, C. Yang, Z. Hou, Y. Zhu, and L. Huang, “Surface corrosion inhibition mechanism of sarcosine as a green novel inhibitor on a novel barrier layer material of cobalt in copper film CMP for GLSI,” *Mater. Sci. Semicond. Process.*, vol. 140, p. 106402, Mar. 2022, doi: 10.1016/J.MSSP.2021.106402.
- [24] A. O. Alnajjar and H. M. Abd El-Lateef, “A novel approach to investigate the synergistic inhibition effect of nickel phosphate nanoparticles with quaternary ammonium surfactant on the Q235-mild steel corrosion: Surface morphology, electrochemical-computational modeling outlines,” *J. Mol. Liq.*, vol. 337, p. 116125, Sep. 2021, doi: 10.1016/J.MOLLIQ.2021.116125.
- [25] F. I. El-Dossoki, M. A. Migahed, M. M. Gouda, and S. A. A. El-Maksoud, “Synergistic enhancing of micellization and thermodynamic properties of some Gemini cationic surfactants related to benzo[d]thiazol-3-ium bromide,” *BMC Chem.*, vol. 18, no. 1, pp. 1–16, Dec. 2024, doi: 10.1186/S13065-024-01334-9/FIGURES/16.
- [26] F. I. El-Dossoki, M. A. Migahed, M. M. Gouda, and S. A. E. H. A. El-Maksoud, “Aggregation behavior of newly synthesized Gemini cationic surfactants in absence and in presence of different inorganic salts in 15% DMSO–water solvent,” *Sci. Reports 2024 141*, vol. 14, no. 1, pp. 1–23, Sep. 2024, doi: 10.1038/s41598-024-69559-1.
- [27] T. A. Hemkemeier, F. C. R. Almeida, A. Sales, and A. J. Klemm, “Corrosion monitoring by open circuit potential in steel reinforcements embedded in cementitious composites with industrial wastes,” *Case Stud. Constr. Mater.*, vol. 16, p. e01042, Jun. 2022.
- [28] J. Tuma Ahmed, “B3LYP/DFT Calculations of Donor- π bridge-Acceptor Molecular System,” *IOSR J. Eng.*, vol. 4, no. 9, pp. 01–08, Sep. 2014, doi: 10.9790/3021-04920108.
- [29] M. Boudalia, R. M. Fernández-Domene, L. Guo, S. Echihi, M. E. Belghiti, A. Zarrouk, A. Bellaouchou, A. Guenbour, and J. García-Antón, “Experimental and Theoretical Tests on the

- Corrosion Protection of Mild Steel in Hydrochloric Acid Environment by the Use of Pyrazole Derivative,” *Materials (Basel)*, vol. 16, no. 2, Jan. 2023, doi: 10.3390/MA16020678.
- [30] D. S. Chauhan, C. Verma, and M. A. Quraishi, “Molecular structural aspects of organic corrosion inhibitors: Experimental and computational insights,” *J. Mol. Struct.*, vol. 1227, p. 129374, Mar. 2021, doi: 10.1016/J.MOLSTRUC.2020.129374.
- [31] V. N. Ayukayeva, G. I. Boiko, N. P. Lyubchenko, R. G. Sarmurzina, R. F. Mukhamedova, U. S. Karabalin, and S. A. Dergunov, “Polyoxyethylene sorbitan trioleate surfactant as an effective corrosion inhibitor for carbon steel protection,” *Colloids Surfaces A Physicochem. Eng. Asp.*, vol. 579, p. 123636, Oct. 2019, doi: 10.1016/J.COLSURFA.2019.123636.
- [32] B. Chugh, A. K. Singh, S. Thakur, B. Pani, A. K. Pandey, H. Lgaz, I. M. Chung, and E. E. Ebenso, “An Exploration about the Interaction of Mild Steel with Hydrochloric Acid in the Presence of N-(Benzo[d]thiazole-2-yl)-1-phenylethan-1-imines,” *J. Phys. Chem. C*, vol. 123, no. 37, pp. 22897–22917, Sep. 2019, doi: 10.1021/ACS.JPCC.9B03994/SUPPL_FILE/JP9B03994_SI_001.PDF.
- [33] S. Arrhenius, “Über die Reaktionsgeschwindigkeit bei der Inversion von Rohrzucker durch Säuren,” *Zeitschrift für Phys. Chemie*, vol. 4U, no. 1, pp. 226–248, Jul. 1889, doi: 10.1515/ZPCH-1889-0416.
- [34] K. J. Laidler and M. C. King, “The development of transition-state theory,” *J. Phys. Chem.*, vol. 87, no. 15, pp. 2657–2664, 1983, doi: 10.1021/J100238A002/ASSET/J100238A002.FP.PNG_V03.
- [35] A. Fawzy and A. Toghan, “Inhibition Evaluation of Chromotrope Dyes for the Corrosion of Mild Steel in an Acidic Environment: Thermodynamic and Kinetic Aspects,” *ACS Omega*, vol. 6, no. 5, pp. 4051–4061, Feb. 2021.
- [36] A. Abd-ElHamid, W. I. A. El-Dougdog, S. M. Syam, I. Aiad, S. M. Shaban, and D. H. Kim, “Synthesis of gemini cationic surfactants-based pyridine Schiff base for steel corrosion and sulfate reducing bacteria mitigation,” *J. Mol. Liq.*, vol. 369, p. 120890, Jan. 2023.
- [37] H. Assad and A. Kumar, “Understanding functional group effect on corrosion inhibition efficiency of selected organic compounds,” *J. Mol. Liq.*, vol. 344, p. 117755, Dec. 2021.
- [38] M. Behpour, S. M. Ghoreishi, N. Soltani, M. Salavati-Niasari, M. Hamadani, and A. Gandomi, “Electrochemical and theoretical investigation on the corrosion inhibition of mild steel by thiosalicylaldehyde derivatives in hydrochloric acid solution,” *Corros. Sci.*, vol. 50, no. 8, pp. 2172–2181, Aug. 2008, doi: 10.1016/J.CORSCI.2008.06.020.
- [39] F. Zhang, X. Li, S. Deng, M. Tang, and G. Du, “Amphoteric surfactant of octadecyl dimethyl betaine as an efficient corrosion inhibitor for cold rolled steel in phosphoric acid solution,” *J. Mater. Res. Technol.*, vol. 15, pp. 7050–7069, Nov. 2021, doi: 10.1016/J.JMRT.2021.11.107.
- [40] E. Ituen, O. Akaranta, and A. James, “Evaluation of Performance of Corrosion Inhibitors Using Adsorption Isotherm Models: An Overview,” *Chem. Sci. Int. J.*, vol. 18, no. 1, pp. 1–34, Jan. 2017, doi: 10.9734/CSJI/2017/28976.
- [41] Z. Szklarska-Smialowska and G. Wieczorek, “Adsorption isotherms on mild steel in H₂SO₄ solutions for primary aliphatic compounds differing in length of the chain,” *Corros. Sci.*, vol. 11, no. 11, pp. 843–852, Jan. 1971, doi: 10.1016/S0010-938X(71)80048-3.
- [42] F. J. Mellenkamp, “Application of Gibbs-Helmholtz Equation to Concentration Cells,” *Phys. Rev. (Series I)*, vol. 29, no. 4, p. 329, Oct. 1909, doi: 10.1103/PhysRevSeriesI.29.329.
- [43] P. B. Petersen and R. J. Saykally, “Confirmation of enhanced anion concentration at the liquid water surface,” *Chem. Phys. Lett.*, vol. 397, no. 1–3, pp. 51–55, Oct. 2004.
- [44] S. S. Shivakumar and K. N. Mohana, “Corrosion Behavior and Adsorption Thermodynamics of Some Schiff Bases on Mild Steel Corrosion in Industrial Water Medium,” *Int. J. Corros.*, vol. 2013, no. 1, p. 543204, Jan. 2013, doi: 10.1155/2013/543204.
- [45] M. P. Chakravarthy, K. N. Mohana, and C. B. Pradeep Kumar, “Corrosion inhibition effect and

- adsorption behaviour of nicotinamide derivatives on mild steel in hydrochloric acid solution,” *Int. J. Ind. Chem.*, vol. 5, no. 2, pp. 1–21, Jun. 2014, doi: 10.1007/S40090-014-0019-3/FIGURES/15.
- [46] B. Krajewska and M. Brindell, “Thermodynamic study of competitive inhibitors’ binding to urease,” *J. Therm. Anal. Calorim.*, vol. 123, no. 3, pp. 2427–2439, Mar. 2016.
- [47] J. T. MacQueen, “Some observations concerning the van’t Hoff equation,” *J. Chem. Educ.*, vol. 44, no. 12, pp. 755–756, 1967, doi: 10.1021/ED044P755.
- [48] M. A. Quraishi, M. Z. A. Rafiquee, S. Khan, and N. Saxena, “Corrosion inhibition of aluminium in acid solutions by some imidazoline derivatives,” *J. Appl. Electrochem.*, vol. 37, no. 10, pp. 1153–1162, Oct. 2007, doi: 10.1007/S10800-007-9379-0/FIGURES/10.
- [49] S. Yahya, N. K. Othman, A. R. Daud, A. Jalar, and R. Ismail, “The influence of temperature on the inhibition of carbon steel corrosion in acidic lignin,” *Anti-Corrosion Methods Mater.*, vol. 62, no. 5, pp. 301–306, Sep. 2015, doi: 10.1108/ACMM-01-2014-1339/FULL/PDF.
- [50] P. Muthukrishnan, B. Jeyaprabha, and P. Prakash, “Adsorption and corrosion inhibiting behavior of *Lanea coromandelica* leaf extract on mild steel corrosion,” *Arab. J. Chem.*, vol. 10, pp. S2343–S2354, May 2017, doi: 10.1016/J.ARABJC.2013.08.011.
- [51] A. M. Al-Sabagh, H. M. Abd-El-Bary, R. A. El-Ghazawy, M. R. Mishrif, and B. M. Hussein, “Corrosion inhibition efficiency of linear alkyl benzene derivatives for carbon steel pipelines in 1M HCl,” *Egypt. J. Pet.*, vol. 20, no. 2, pp. 33–45, Jun. 2011, doi: 10.1016/J.EJPE.2011.06.010.
- [52] N. H. Alharthi, M. A. El-Hashemy, W. M. Derafa, I. O. Althobaiti, and H. A. Altaleb, “Corrosion inhibition of mild steel by highly stable polydentate schiff base derived from 1,3- propanediamine in aqueous acidic solution,” *J. Saudi Chem. Soc.*, vol. 26, no. 4, p. 101501, Jul. 2022, doi: 10.1016/J.JSCS.2022.101501.
- [53] K. Kiruthikajothi and G. Chandramohan, “Corrosion inhibition of mild steel in hydrochloric acid solution by amino acid complexes,” *Orient. J. Chem.*, vol. 31, no. 3, pp. 1351–1354, 2015, doi: 10.13005/OJC/310312.
- [54] M. Farsak, H. Keleş, and M. Keleş, “A new corrosion inhibitor for protection of low carbon steel in HCl solution,” *Corros. Sci.*, vol. 98, pp. 223–232, Sep. 2015, doi: 10.1016/J.CORSCI.2015.05.036.
- [55] N. Esmaili, J. Neshati, and I. Yavari, “Corrosion inhibition of new thiocarbonylhydrazides on the carbon steel in hydrochloric acid solution,” *J. Ind. Eng. Chem.*, vol. 22, pp. 159–163, Feb. 2015, doi: 10.1016/J.JIEC.2014.07.004.
- [56] S. A. A. A. El-Maksoud, F. I. I. El-Dossoki, M. A. A. Migahed, and M. M. M. Gouda, “Impact of Some Novel Synthesized Cationic Surfactants on the Corrosion of Carbon Steel in 1M HCl Solutions,” *J. Mater. Eng. Perform.*, vol. 30, no. 5, pp. 3845–3858, May 2021.
- [57] S. C. Joycee, A. S. Raja, A. S. Amalraj, and S. Rajendran, “Inhibition of corrosion of mild steel pipeline carrying simulated oil well water by *Allium sativum* (Garlic) extract,” *Int. J. Corros. Scale Inhib.*, vol. 10, no. 3, pp. 943–960, 2021, doi: 10.17675/2305-6894-2021-10-3-8.
- [58] M. Larif, A. Elmidaoui, A. Zarrouk, H. Zarrok, R. Salghi, B. Hammouti, H. Oudda, and F. Bentiss, “An investigation of carbon steel corrosion inhibition in hydrochloric acid medium by an environmentally friendly green inhibitor,” *Res. Chem. Intermed.*, vol. 39, no. 6, pp. 2663–2677, Jul. 2013, doi: 10.1007/S11164-012-0788-2/TABLES/6.
- [59] H. Ashassi-Sorkhabi, D. Seifzadeh, and M. G. Hosseini, “EN, EIS and polarization studies to evaluate the inhibition effect of 3H-phenothiazin-3-one, 7-dimethylamin on mild steel corrosion in 1 M HCl solution,” *Corros. Sci.*, vol. 50, no. 12, pp. 3363–3370, Dec. 2008, doi: 10.1016/J.CORSCI.2008.09.022.
- [60] F. Teymouri, S. R. Allahkaram, M. Shekarchi, I. Azamian, and M. Johari, “A comprehensive study on the inhibition behaviour of four carboxylate-based corrosion inhibitors focusing on efficiency drop after the optimum concentration for carbon steel in the simulated concrete pore solution,” *Constr. Build. Mater.*, vol. 296, p. 123702, Aug. 2021, doi: 10.1016/J.CONBUILDMAT.2021.123702.

- [61] V. Vivier and M. E. Orazem, "Impedance Analysis of Electrochemical Systems," *Chem. Rev.*, vol. 122, no. 12, pp. 11131–11168, Jun. 2022.
- [62] M. J. Gimeno, S. Chamorro, R. March, E. Oró, P. Pérez, J. Gracenea, and J. Suay, "Anticorrosive properties enhancement by means of phosphate pigments in an epoxy 2k coating. Assessment by NSS and ACET," *Prog. Org. Coatings*, vol. 77, no. 12, pp. 2024–2030, Dec. 2014, doi: 10.1016/J.PORGCOAT.2014.04.004.
- [63] W. Emori, S. L. Jiang, D. L. Duan, and Y. G. Zheng, "Effects of Sodium Thiosulfate and Sodium Sulfide on the Corrosion Behavior of Carbon Steel in an MDEA-Based CO₂ Capture Process," *J. Mater. Eng. Perform.*, vol. 26, no. 1, pp. 335–342, Jan. 2017, doi: 10.1007/S11665-016-2458-9/METRICS.
- [64] M. H. Sliem, A. B. Radwan, F. S. Mohamed, N. A. Alnuaimi, and A. M. Abdullah, "An efficient green ionic liquid for the corrosion inhibition of reinforcement steel in neutral and alkaline highly saline simulated concrete pore solutions," *Sci. Reports 2020 101*, vol. 10, no. 1, pp. 1–15, Sep. 2020, doi: 10.1038/s41598-020-71222-4.
- [65] S. Pruneanu, A. Boughriet, A. Henderson, C. Malins, Z. Ali, and L. Olenic, "Impedimetric measurements for monitoring avidin-biotin interaction on self-assembled monolayer," *Part. Sci. Technol.*, vol. 26, no. 2, pp. 136–144, 2008, doi: 10.1080/02726350801890870.
- [66] M. te Vrugt, H. Löwen, and R. Wittkowski, "Classical dynamical density functional theory: from fundamentals to applications," *Adv. Phys.*, vol. 69, no. 2, pp. 121–247, Apr. 2020, doi: 10.1080/00018732.2020.1854965.
- [67] A. Kokalj, "On the alleged importance of the molecular electron-donating ability and the HOMO–LUMO gap in corrosion inhibition studies," *Corros. Sci.*, vol. 180, p. 109016, Mar. 2021, doi: 10.1016/J.CORSCI.2020.109016.
- [68] A. Kokalj, C. Xie, I. Milošev, and D. Crespo, "How relevant are molecular electronic parameters for predicting corrosion inhibition efficiency: imidazoles as corrosion inhibitors of Cu/Zr materials in NaCl solution," *Corros. Sci.*, vol. 193, p. 109900, Dec. 2021, doi: 10.1016/J.CORSCI.2021.109900.
- [69] D. M. Mamand and H. M. Qadr, "Corrosion inhibition efficiency and quantum chemical studies of some organic compounds: theoretical evaluation," *Corros. Rev.*, vol. 41, no. 4, pp. 427–441, Aug. 2023, doi: 10.1515/CORREX-2022-0085/DOWNLOADASSET/SUPPL/J_CORREX-2022-0085_SUPPL_001.DOCX.
- [70] S. Kaya, B. Tüzün, C. Kaya, and I. B. Obot, "Determination of corrosion inhibition effects of amino acids: Quantum chemical and molecular dynamic simulation study," *J. Taiwan Inst. Chem. Eng.*, vol. 58, pp. 528–535, Jan. 2016, doi: 10.1016/J.JTICE.2015.06.009.
- [71] A. Zarrouk, B. Hammouti, A. Dafali, M. Bouachrine, H. Zarrok, S. Boukhris, and S. S. Al-Deyab, "A theoretical study on the inhibition efficiencies of some quinoxalines as corrosion inhibitors of copper in nitric acid," *J. Saudi Chem. Soc.*, vol. 18, no. 5, pp. 450–455, Nov. 2014, doi: 10.1016/J.JSCS.2011.09.011.
- [72] A. Belkheiri, K. Dahmani, K. Mzioud, M. Khattabi, O. Kharbouch, M. Galai, Y. Merroun, N. Dkhireche, Z. Benzekri, S. Boukhris, R. Almeer, A. Chaouiki, and M. E. Touhami, "Assessment of 14-(4-nitrophenyl)-14H-dibenzo[a,j]xanthene as an effective organic corrosion inhibitor for mild steel in 1 M HCl: Electrochemical, theoretical, and surface analysis," *Int. J. Electrochem. Sci.*, vol. 20, no. 1, p. 100907, Jan. 2025, doi: 10.1016/J.IJOES.2024.100907.
- [73] O. S. Shehata, L. A. Khorshed, and H. S. Mandour, "Effect of Acetamide Derivative and its Mn-Complex as Corrosion Inhibitor for Mild Steel in sulphuric Acid," *Egypt. J. Chem.*, vol. 60, no. 2, pp. 243–259, Apr. 2017, doi: 10.21608/EJCHEM.2017.674.1014.
- [74] B. Zhang, C. He, X. Chen, Z. Tian, and F. Li, "The synergistic effect of polyamidoamine

- dendrimers and sodium silicate on the corrosion of carbon steel in soft water,” *Corros. Sci.*, vol. 90, pp. 585–596, Jan. 2015, doi: 10.1016/J.CORSCI.2014.10.054.
- [75] H. Liu, C. Chen, X. Yuan, Y. Tan, G. Meng, H. Liu, and Y. F. Cheng, “Corrosion inhibition behavior of X80 pipeline steel by imidazoline derivative in the CO₂-saturated seawater containing sulfate-reducing bacteria with organic carbon starvation,” *Corros. Sci.*, vol. 203, p. 110345, Jul. 2022, doi: 10.1016/J.CORSCI.2022.110345.
- [76] A. M. Ridhwan, A. A. Rahim, and A. M. Shah, “Synergistic Effect of Halide Ions on the Corrosion Inhibition of Mild Steel in Hydrochloric Acid using Mangrove Tannin,” *Int. J. Electrochem. Sci.*, vol. 7, no. 9, pp. 8091–8104, Sep. 2012, doi: 10.1016/S1452-3981(23)17978-8.
- [77] S. A. Umoren and M. M. Solomon, “Synergistic corrosion inhibition effect of metal cations and mixtures of organic compounds: A Review,” *J. Environ. Chem. Eng.*, vol. 5, no. 1, pp. 246–273, Feb. 2017, doi: 10.1016/J.JECE.2016.12.001.
- [78] S. Huang, P. Du, C. Min, Y. Liao, H. Sun, and Y. Jiang, “Poly(1-amino-5-chloroanthraquinone): Highly Selective and Ultrasensitive Fluorescent Chemosensor for Ferric Ion,” *J. Fluoresc.*, vol. 23, no. 4, pp. 621–627, Jul. 2013, doi: 10.1007/S10895-013-1179-9.
- [79] H. Bairagi, P. Vashishth, G. Ji, S. K. Shukla, E. E. Ebenso, and B. Mangla, “Polymers and their composites for corrosion inhibition application: Development, advancement, and future scope—A critical review,” *Corros. Commun.*, vol. 15, pp. 79–94, Sep. 2024.
- [80] P. Rodič, M. Može, I. Golobič, and I. Milošev, “Functionalisation of the Aluminium Surface by CuCl₂ Chemical Etching and Perfluoro Silane Grafting: Enhanced Corrosion Protection and Improved Anti-Icing Behaviour,” *Met. 2024, Vol. 14, Page 1118*, vol. 14, no. 10, p. 1118, Oct. 2024, doi: 10.3390/MET14101118.
- [81] K. F. Khaled and S. S. Abdel-Rehim, “Electrochemical investigation of corrosion and corrosion inhibition of iron in hydrochloric acid solutions,” *Arab. J. Chem.*, vol. 4, no. 4, pp. 397–402, Oct. 2011, doi: 10.1016/J.ARABJC.2010.07.006.
- [82] H. M. Abd El-Lateef and M. M. Khalaf, “Synergistic inhibition effect of novel counterion-coupled surfactant based on rice bran oil and halide ion on the C-steel corrosion in molar sulphuric acid: Experimental and computational approaches,” *J. Mol. Liq.*, vol. 331, p. 115797, Jun. 2021, doi: 10.1016/J.MOLLIQ.2021.115797.
- [83] S. A. Xavier Stango and U. Vijayalakshmi, “Studies on corrosion inhibitory effect and adsorption behavior of waste materials on mild steel in acidic medium,” *J. Asian Ceram. Soc.*, vol. 6, no. 1, pp. 20–29, 2018, doi: 10.1080/21870764.2018.1439608.
- [84] Y. Liu, C. Huang, H. Yang, X. Sun, H. Zhang, Y. Sun, W. Zhang, H. Lan, and S. Yu, “Enhanced Corrosion Resistance of CuAl/BN Coatings through the Addition of Rare Earth Elements and High-Temperature Oxidation Treatment,” *Cryst. 2024, Vol. 14, Page 808*, vol. 14, no. 9, p. 808, Sep. 2024, doi: 10.3390/CRYST14090808.
- [85] D. Lundberg, “The coordination chemistry of solvated metal ions in DMPU: a study of a space-demanding solvent,” *Acta Univ. Agric. Sueciae*, no. 2006:23, 2006, Accessed: Jan. 14, 2024.